11-2011

Prospects for Nanowire-Doped Polycrystalline Graphene Films for Ultratransparent, Highly Conductive Electrodes

Changwook Jeong
Purdue University, jeongc@purdue.edu

Pradeep Nair
Purdue University, pnair@purdue.edu

Mohammad Khan
Purdue University

Mark Lundstrom
Purdue University, lundstro@purdue.edu

Muhammad Alam
Purdue University, alam@purdue.edu

Jeong, Changwook; Nair, Pradeep; Khan, Mohammad; Lundstrom, Mark; and Alam, Muhammad, "Prospects for Nanowire-Doped Polycrystalline Graphene Films for Ultratransparent, Highly Conductive Electrodes" (2011). *Birck and NCN Publications.* Paper 839.
http://dx.doi.org/10.1021/nl203041n

NANO LETTERS

LETTER

pubs.acs.org/NanoLett

Prospects for Nanowire-Doped Polycrystalline Graphene Films for Ultratransparent, Highly Conductive Electrodes

Changwook Jeong,* Pradeep Nair, Mohammad Khan, Mark Lundstrom, and Muhammad A. Alam*

Network for Computational Nanotechnology, Birck Nanotechnology Center, Purdue University, West Lafayette, Indiana 47907, United States

Supporting Information

ABSTRACT: Traditional transparent conducting materials such as ITO are expensive, brittle, and inflexible. Although alternatives like networks of carbon nanotubes, polycrystalline graphene, and metallic nanowires have been proposed, the transparency-conductivity trade-off of these materials makes them inappropriate for broad range of applications. In this paper, we show that the conductivity of polycrystalline graphene is limited by high resistance grain boundaries. We demonstrate that a composite based on polycrystalline graphene and a subpercolating network of metallic nanowires offers a simple and effective route to reduced resistance while maintaining high transmittance. This new approach of "percolation-doping by nanowires" has the potential to beat the transparency-conductivity constraints of existing materials and may be suitable for broad applications in photovoltaics, flexible electronics, and displays.

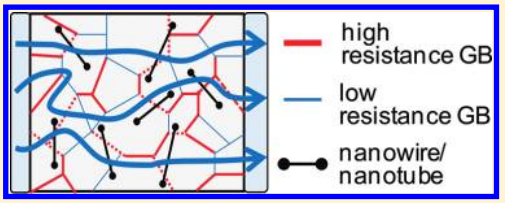

KEYWORDS: Graphene, nanowires, electrode, flexible, transparent, percolation

Since resistivity and transmittance are often fundamentally constrained by the intrinsic properties of a material, developing transparent conducting materials (TCMs) with low sheet resistance (R_S < 10 Ω/sq) and high transmittance (T > 90%) has been a persistent challenge. Different metal-doped oxides such as indium tin oxide (ITO) are widely used in commercial applications, but a replacement for ITO is desired for the following reasons:[1] (1) the limited availability and high cost of indium, (2) increasing brittleness with aging, (3) chemical instability under acid or base conditions, (4) poor transmittance in the near-infrared region,[2] and (5) metallic−ion diffusion from ITO into thin barrier layers that results in parasitic leakage.[3] These problems make ITO-based technologies, such as thin-film photovoltaics (PV), touch-screen displays, light emitting diodes, etc., expensive. Various alternative TCMs, such as networks of carbon nanotubes (CNT)[4,5] or metal nanowires (NW)[6,7] and chemical vapor deposited (CVD) polycrystalline graphene (polygraphene),[8−11] have also been explored. While these potential ITO replacements resolve several practical issues associated with ITO, Figure 1 suggests that their respective R_S−T curves are not significantly different than that of ITO. To understand why, consider the constraints of random CNT or metallic NW networks. To achieve technologically relevant values of R_S < 20 Ω/sq,[6] the density of NWs or CNTs must significantly exceed the percolation threshold for higher sheet conductance;[12] such high density however reduces the transmittance considerably.[6,13] Moreover, even with low R_S, the vertical current collection in PV cells is compromised by current crowding at the small-area interface between nanotubes/nanowire electrode and the bulk emitter layer.[12] Graphene provides another intriguing option; *four* layers of CVD graphene, fabricated by a roll-to-roll process, has already shown R_S ∼ 30 Ω/sq and T ∼ 90%.[8] Available experimental data,[14] however, suggest that there is a fundamental limitation in sheet resistance and transmittance of thin graphene film and that it may be difficult for polycrystalline graphene to compete successfully with ITO.[13]

In this paper, we use an experimentally calibrated, comprehensive numerical model for electron transport in polycrystalline graphene to conclude that the high resistivity of the film reflects an intrinsic percolation bottleneck of the system in which electrons are periodically trapped in domains formed by high-resistance grain boundaries (GBs). A novel concept which "dopes" polygraphene with metallic nanowires can overcome this transport bottleneck to achieve T > 90% and R_S < 20 Ω/sq, with performance comparable to or better than that of ITO. To distinguish the effects of doping by metallic NWs from those by standard chemical or electrostatic techniques, we define a concept that we call "percolation-doping": a *positive* percolation-doping by metallic nanowires improves conductivity not by increasing the free carrier density but rather by increasing the number of electronic pathways to bridge the percolation bottleneck. A *negative* percolation doping—in the form of striping of nanotube network—has been previously used in a different context.[15,35] The continuity of polygraphene ensures vertical current collection free from current crowding, and a small footprint of nanowires on graphene film ensures that high optical transmittance of single layer graphene is not compromised by percolation-doping.

The paper is organized as follows. To explore the origin of high R_S in polygraphene films, we first construct microstructures

Received: September 1, 2011
Published: October 10, 2011

dx.doi.org/10.1021/nl203041n | *Nano Lett.* 2011, 11, 5020–5025

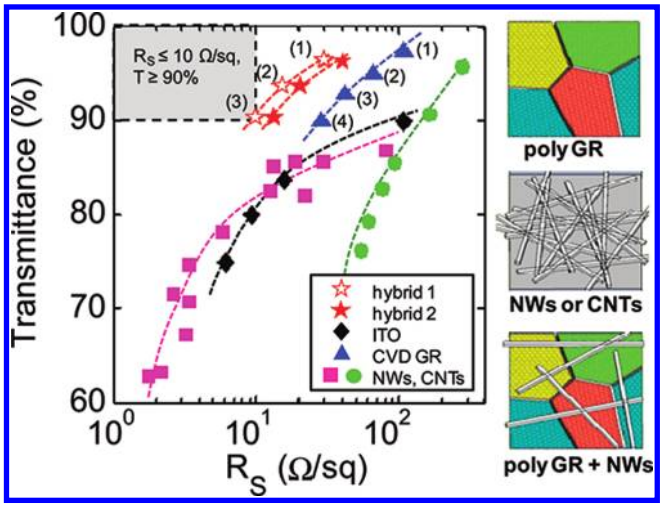

Figure 1. Transmittance as a function of sheet resistance (R_S) for polycrystalline graphene grown by the chemical vapor deposition (CVD) method,[8] the networks of carbon nanotubes (CNTs)[5] and nanowires (NWs),[6] ITO,[8] and a hybrid of polygraphene and NW mesh. The dashed lines are a guide for the eye. The best reported data are selected from the literature. The data for the hybrid are computed based on the following parameters: the R_S of a single crystalline graphene ~30 Ω/sq, the ratio of intergrain resistance to intragrain resistance ~63, the percentage of high-resistance grain boundary (P_{GB}) = 35%, the contact resistance between metal NW and graphene (R_C) = 20 Ω · μm (hybrid 1) and R_C = 200 Ω · μm (hybrid 2), and geometric aperture of 99% (an average distance between NWs of ~10 μm, a line width of 100 nm, and a height of 100 nm) for metal NW mesh with bulk Ag conductivity being assumed. The value in the bracket represents the number of layers for polygraphene or the hybrid.

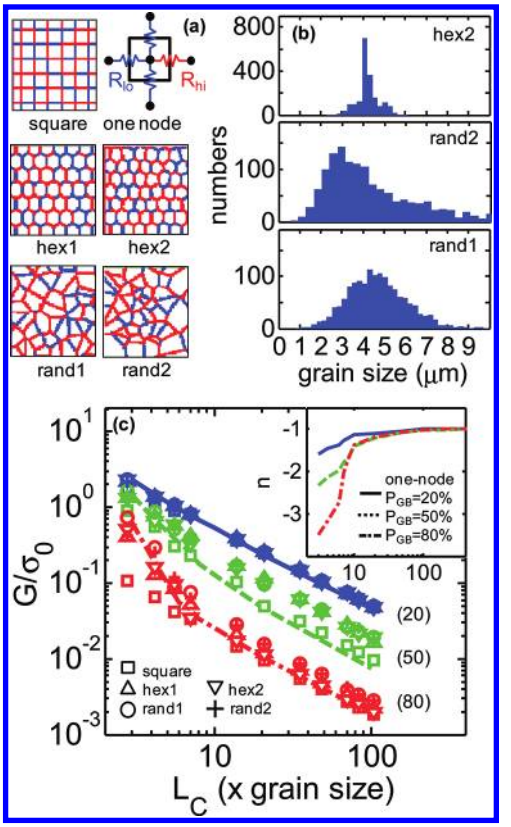

Figure 2. (a) Five microstructures generated by Voronoi tessellation for use of finite difference method: uniform square grain (square), uniform hexagonal grain (hex1), perturbed hexagonal grain with normal size distribution (hex2), and random grains with normal size distribution (rand1) and with log-normal size distribution (rand2). The percentage of high-resistance grain boundary is 50%. High- and low- resistance grain boundaries are shown by red and by blue lines. A grain is shown by white and has about 200 nodes per grain. A schematic diagram for one model is also shown to explain how the one-node model represents one grain. The sheet resistance across low-resistance grain boundary and the sheet resistance across high resistance grain boundary are denoted as R_{lo} and R_{hi}, respectively. (b) Grain size distributions are shown for perturbed hexagonal grain and two random grains. (c) The normalized conductance vs sample length for five different microstructures (symbols) and one-node model (solid, dashed, and dashed-dot line) for three different percentages of high-resistance GB (P_{GB} = 20%, 50%, and 80%). Inset: the dependence of the conductance exponent, n, on the sample length, i.e., $G \propto (L_C)^n$.

of typical polygraphene films reported in the literature and calculate their corresponding transport properties. Next, we examine quantitatively the impact of GBs on polycrystalline graphene to demonstrate the importance of a percolation bottleneck in these films. Finally, we propose a hybrid of polycrystalline graphene and a metal NW mesh to improve the performance in terms of R_S and T as well as to reduce variations among samples. Finally, we summarize our conclusions.

Approach. To understand why polygraphene is so resistive, we use a process model to produce representative structures, an electrical model to compute the sheet resistance, and an optical model to compute the transmittance. The modeling approach is described in detail in the Supporting Information. In brief, we begin by synthetically generating polycrystalline graphene samples using Voronoi tessellation.[16] Five types of microstructures (see Figure 2a) of increasing complexity are as follows: (1) uniform square grain as a reference, (2) uniform hexagonal grains to approximate films produced by the seeded growth method,[17] (3) perturbed hexagonal grains with Gaussian size distributions, typical of films produced by seeded growth method,[17] (4) random grains with normal size distribution to represent films produced by CVD graphene,[18] and (5) grains with log-normal size distribution characteristic of CVD graphene.[18,19] The average grain size ($\langle L_{grain} \rangle$) is ~5 μm, consistent with reported values.[9,17] Corresponding grain size distributions are shown in Figure 2b. *Several hundred samples* are prepared for a statistical study of the transport characteristics of the film.

The two key electrical parameters are the resistances of the grains and grain boundaries. In polygraphene, it is experimentally observed that the ratio of the intergrain to intragrain resistance ranges from ~1 to ~30.[17] Although there might be a distribution of GB resistances as a function of misorientation between neighboring grains, for simplicity in the following discussion, we classify the GBs as either a high-resistance GB or a low-resistance GB. To describe electronic transport through the microstructure, we use a drift-diffusion formulation, i.e., $J = \sigma\nabla(F_n/q)$ where J is the current density in A/m, σ the sheet conductivity, and F_n is the electrochemical potential. A drift-diffusion formulation is appropriate for this problem because average grain size (~5 μm) is much larger than the typical mean-free path of hundreds of nanometers.[17,20] (A similar drift-diffusion based approach has also been used for CNT networks, with excellent results.[15]) We assume that the charge current is conserved (i.e., no recombination generation) and solve $\nabla \cdot J = 0$.

dx.doi.org/10.1021/nl203041n |*Nano Lett.* 2011, 11, 5020–5025

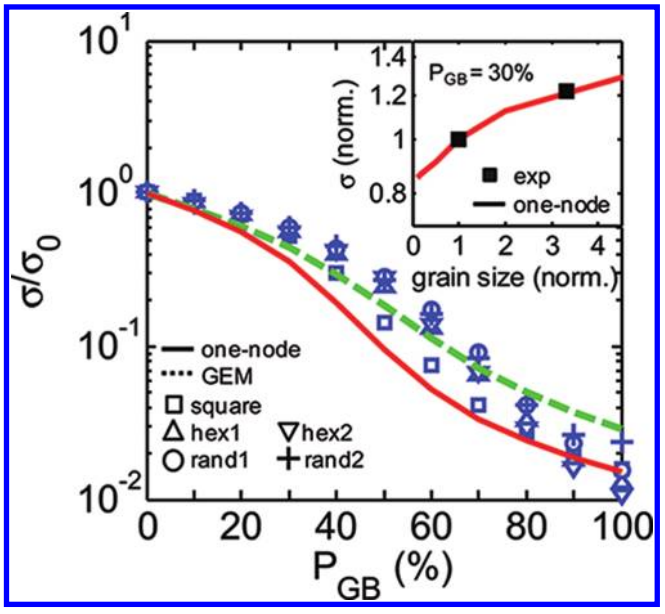

Figure 3. For a long sample ($L_C \sim 100\times$ average grain size), the dependence of the sheet conductance on the percentage of high-resistance grain boundary (P_{GB}) is plotted. Inset: the computed results for grain size dependence are compared to experiments.[9]

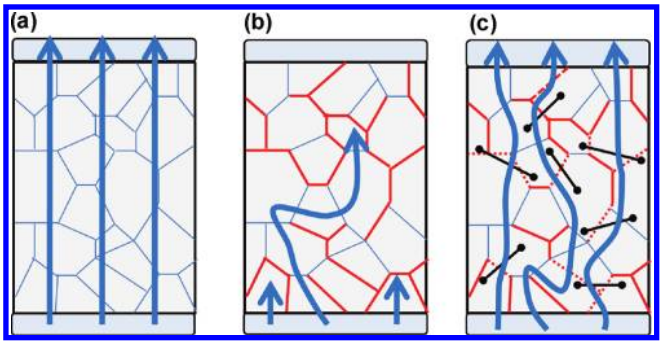

Figure 4. The schematic figures to interpret the resistance of polygraphene as a percolation problem defined by high and low resistance grain boundaries (GB). High-resistance and low-resistance GBs are shown by red and blue lines. (a) P_{GB} = 0%; (b) P_{GB} ~60%; (c) the concept of "percolation-doping": doping the polycrystalline graphene by a sparse random mesh of metal NW. Metal NW is represented by a black solid line. All arrows indicate current stream.

Within the bulk of the polygraphene grain, $\sigma = \sigma_0$. The theoretical lower limit of conductivity is 30 Ω/sq, which occurs when only acoustic deformation potential scattering is present.[36] For the conductivity across a GB, we follow a recent theoretical study,[21] which characterizes a high-resistance GB by transport energy gap (E_G) below which charge carriers are perfectly reflected (i.e., $\sigma_{GB}^{(hi)} < \sigma_0$). A low-resistance GB is taken to be being perfectly transparent (i.e., $\sigma_{GB}^{(lo)} \equiv \sigma_0$.) With these three conductivities, i.e., σ_0, $\sigma_{GB}^{(lo)}$, $\sigma_{GB}^{(hi)}$ the transport problem is fully defined. This model with high- and low- resistance GBs leads to a maze-like morphology landscape through which the electron injected from one contact travels to the other contact, *thereby transforming the problem of transport in polycrystalline graphene into a percolation problem*.

For a given microstructure, the finite difference method (FDM) is used to calculate transport properties. Each grain has about 200 nodes or grid points. The input parameters used for the FDM calculations are the sheet resistance within the grains, $R_{lo} \sim 30$ Ω/sq and the sheet resistance across high-resistance GBs, $R_{hi} \sim 63R_{lo}$. (By assuming the lower limit sheet resistance for the grain, R_{lo}, our results establish the best case performance for large area polycrystalline graphene.) The FDM results are compared to a simple "one-node model", for which each grain is represented by only one node, i.e. by four resistors as shown in Figure 2a. This one-node model is of practical importance because the resistance, including high- or low-resistance GB in the one-node model, can be easily measured.[17] Finally, we calculate the optical transmittance of the system by (numerically) solving Maxwell equations with Floquet periodic boundary condition.[22] Normal illumination was assumed, and the transmittance of both TE and TM waves was calculated for a set of wavelengths spanning the entire solar spectrum.

In Figure 2c, we plot the normalized sheet conductance (for five different microstructures) as a function of length for three different percentages of high-resistance GBs (P_{GB} = 20%, 50%, and 80%). The width of the sample is fixed at 7× average grain size, $\langle L_{grain} \rangle$ after which the width dependence of the transport properties disappears (as should be the case for large area films). The inset of Figure 2c shows the dependence of the conductance exponent, n, on the length, i.e., $G \propto (L_C)^n$.[37] If the length is smaller than ~10× average grain size ($\langle L_{grain} \rangle$), the exponent becomes significantly larger than −1.0, indicating a nonlinear dependence on sample length. Compared to a long sample, there is a higher probability in a short sample that low-resistance GBs and grains form a continuous network between contacts. We are, however, interested in transport in large area (~square meters) polygraphene appropriate for PV applications, where regardless of P_{GB}, the exponent approaches −1.0 with increasing length. *Remarkably, we find that the grain shape and grain size distributions have little effect on the conductance*. This is because it is the average size of the grain and the percentage of the high-resistance GBs and not the specific details of grain-size distributions that dictate the overall transport property of the network.

The plot of normalized conductivity versus percentage of high-resistance GB shown in Figure 3 is characterized by dramatic suppression of conductivity—even for small increase in P_{GB}. This result can be understood with reference to Figure 4, which interprets the resistance of polygraphene as a percolation problem defined by high- and low- resistance GBs. Recall that the percolation threshold for the Voronoi tessellation is (0.667−0.68),[23,24] while that of the hexagonal lattice is 0.6527.[25] Therefore, regardless the specific form of the GB distribution, when the fraction of high-resistance GB approaches ~0.66 (i.e., $P_{GB} \sim$ 66%), electrons traveling between a pair of contacts must cross one (Stanley's red bonds[26]) or more high-resistance GBs; see Figure 4b. This percolation bottleneck suppresses conductivity exponentially.

To support this percolation hypothesis quantitatively, we interpret the numerical results by the generalized effective media (GEM) theory.[27,28] The GEM equation is given by

$$f_{GB}\frac{\sigma_{GB}^{1/t} - \sigma^{1/t}}{\sigma_{GB}^{1/t} + A\sigma^{1/t}} + (1 - f_{GB})\frac{\sigma_0^{1/t} - \sigma^{1/t}}{\sigma_0^{1/t} + A\sigma^{1/t}} = 0 \qquad (1)$$

where f_{GB} is area fraction of grain boundaries, $\sigma_{0(GB)}$ the conductivity of the grain (grain boundary), t a characteristic exponent defined in $\sigma \propto (1 - f_{GB}/f_{C,CB})^t$ with $f_{C,GB}$ being the threshold area fraction of GBs, and the constant A is $A = f_{C,GB}/(1 - f_{C,GB})$. When $\sigma_0/\sigma_{GB} = \infty$, eq 1 is reduced to a form of percolation

dx.doi.org/10.1021/nl203041n |*Nano Lett.* 2011, 11, 5020–5025

equation $\sigma \propto (1 - f_{GB}/f_{C,GB})^t$. With $t = 1$ and $A = 2$, the GEM equation is also reduced to Bruggeman's symmetric effective medium equation.[27] To fit our simulation results, two parameters need to be determined: t and $f_{C,GB}$. We set the bounds for the critical exponent to be from 1.05 to 1.37, typical for 2D bond percolation,[29,30] while $f_{C,GB}$ is adjusted to fit the data. The relation of $f_{C,GB}$ to $P_{C,GB}$ is $P_{C,GB} = f_{C,GB}(P_{GB}^{100\%}/f_{GB}^{100\%})$, where $f_{GB}^{100\%} \sim 12.6\%$ is the area fraction of GB when $P_{GB} = 100\%$ (in the FDM simulation). The intensity of D bands in the spectroscopic Raman mapping of graphene grains and grain boundaries showed $f_{GB}^{100\%} \sim 10\%$.[17] As shown by the dashed line in Figure 3, our numerical results for polygraphene transport are well-reproduced by the GEM equation when $t = 1.05$ and $f_{C,CB} = 8.4 \pm 0.2\%$ corresponding to a percolation threshold of P_{GB}, $P_{C,CB} = 67 \pm 1.6\%$, almost *precisely the value expected from the percolation-hypothesis that interprets polygraphene transport in terms of percolative transport on Voronoi tessellation*[23,24] *and hexagonal honeycomb lattice*.[25]

Having established the validity of the theory, it can now be used to explain why polygraphene is so resistive and to extract P_{GB} from experimental data. For example, the inset of Figure 3 compares the computed grain size dependence of sheet conductance to experiments. With the assumption of $R_{hi} \sim 60R_{lo}$, we find $P_{GB} \approx 30\%$ gives a good match between our model and experiments. For this $P_{GB} < P_{C,GB}$, the effect of grain boundaries is still significant and percolative transport plays an important role in defining sheet conductivity, with $\sigma/\sigma_0 > 0.2-0.3$.

NW-Doped Polygraphene. The results discussed above show that the key to reduce sheet resistance of polygraphene is either by increasing grain size or by reducing the number of high-resistance grain boundaries. Even if the grain size could be further enlarged by various process techniques,[9,17] these grains will be always smaller than the dimension of transparent conductors necessary for PV applications. Most importantly, there is no obvious approach to control the magnitude or the number of high-resistance grain boundaries by simple process changes. Clearly, a more practical technique to alleviate the influence of high-resistance GBs is needed for graphene electrodes to be competitive with ITO.

To decrease the influence of high-resistance GBs, we propose (see Figure 4c) a novel concept which "dopes" the polycrystalline graphene with a sparse random mesh of metal NWs. The density of these nanowires should be below the percolation threshold, so that *NW−NW connectivity is not expected and the NWs themselves do not form a percolating network (Figure 4c, black lines).* If the nanowire length is larger than that of the grain, the NWs will cross the grain boundaries with probability approaching 1. If a NW intersects a high-resistance grain boundary, the GB can no longer inhibit current conduction, so that effective P_{GB} is reduced (see Figure 4c). Given the exponential dependence of conductance on P_{GB}, even a modest percolation-doping by metallic NW can dramatically decrease the R_S of polygraphene films. The following example illustrates our proposition.

To examine the effectiveness of NW doping, consider a polygraphene film with average grain size of 5 μm decorated with a random dispersion of ~8 μm long, 100 nm diameter Ag nanowires.[6] These Ag NWs will bridge the neighboring grains with probability approaching 1. The NW density (ρ_{NW}) is varied from 0 to 100%. We define the 100% coverage when the average distance between NWs is ~8−10 μm, so that every other grain—on average—contains a NW. For samples with ρ_{NW} <100%, the proportional fraction of NWs are randomly removed. On the basis of a recent measurement,[31] the contact resistance between

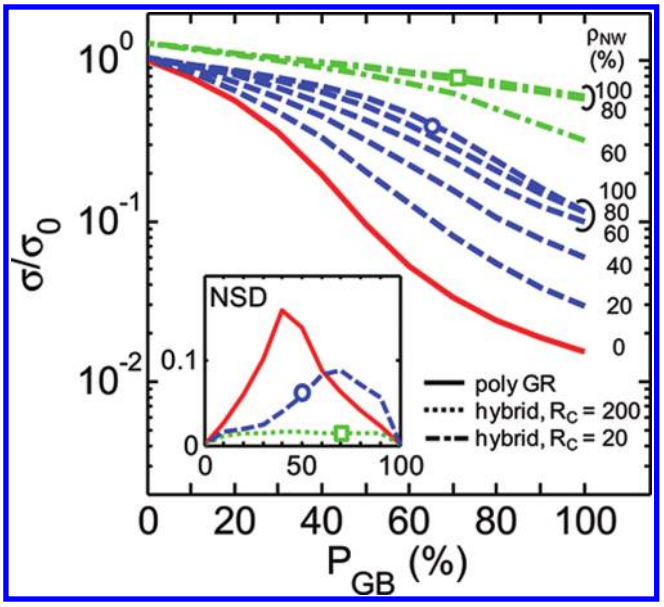

Figure 5. For a hybrid of polycrystalline graphene (poly-GR) and nanowire (NW) mesh, the sheet conductance vs the percentage of high-resistance grain boundaries (P_{GB}) for two different contact resistances (R_C) are plotted as a function of NW density (ρ_{NW}). At ρ_{NW} = 100%, average distance between NWs is ~10 μm and ρ_{NW} = 0% represents poly-GR. Inset: the normalized standard deviation (NSD) is plotted.

metal and graphene is $R_C \sim 200\ \Omega\cdot\mu$m. The theoretical lower limit of $R_C \approx 20\ \Omega\cdot\mu$m[32] is obtained by assuming that the work function (W) difference between graphene and silver is about 0.3 eV ($W_{graphene}$ = 4.4−4.6 eV, W_{Ag} = 4.7−4.9 eV).[33] The polygraphene conductivities remain unchanged.

Two-dimensional simulation of NW-doped graphene can now be used to calculate the overall conductivity, σ, of the NW-doped polygraphene film. The results are summarized in Figure 5. The red solid line represents the normalized conductivity of polygraphene without NW-doping (ρ_{NW} = 0%). From this curve, the best reported sheet resistance of monolayer CVD graphene[8] of 125 Ω/sq translates to $P_{GB} \approx 35\%$—a typical value. As we increase the NW density, the conductivity increases dramatically—even with a sparse network of only 60% coverage (one NW for every four grains) and relatively poor $R_C \approx 200\ \Omega\cdot\mu$m, the sheet conductance σ begins to approach that of pure single crystalline graphene $R_S \sim 30\ \Omega$/sq. Obviously, the conductivity improves further for lower contact resistance (i.e., $R_C \approx 20\ \Omega\cdot\mu$m) as the quasi-percolating NWs begin to carry a larger fraction of the current between the contacts and σ reduces below 30 Ω/sq. Given that the sheet resistance of a monolayer of a graphene−NW hybrid, the sheet resistance of two to three layers of the NW-doped graphene film is obtained by $R_{S,hybrid}^{n(=2-3)} = R_{S,hybrid}^{1}/n(=2-3)$. This linear dependency of R_S was also observed for roll-to-roll processed CVD graphene.[8] Indeed, as shown in Figure 1, a stack consisting of two to three layers of the NW-doped graphene offers sheet resistance approaching 10 Ω/sq—the conductivity target for the potential replacement of ITO.

To understand how NW doping achieves this dramatic improvement, let us consider an illustrative example. In panels a−f of Figure 6 we compare the FDM calculation of polycrystalline graphene sample with $P_{GB} \approx 35\%$ to that of hybrid polycrystalline graphene−metal NWs in terms of the potential profile. Note that network of metal NWs is sparse enough not to

dx.doi.org/10.1021/nl203041n |*Nano Lett.* 2011, 11, 5020–5025

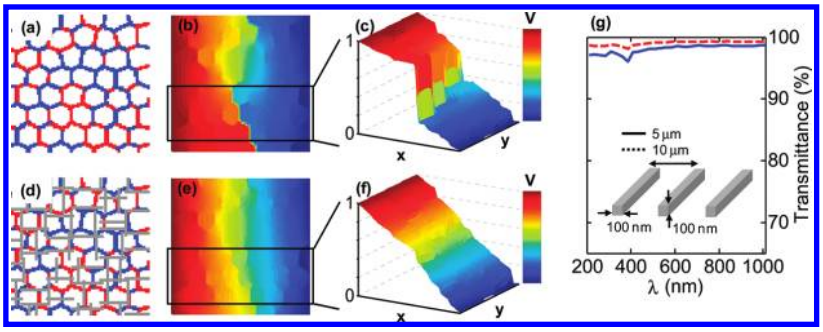

Figure 6. (a) A polycrystalline graphene sample with perturbed hexagonal grain for P_{GB} = 35%. High-resistance and low-resistance grain boundaries (GB) are shown by red and blue lines, respectively. (d) Hybrid polycrystalline graphene network of metal NWs (gray solid line). (b, c, e, f) Corresponding potential profiles are plotted for comparison. All potential data are normalized. The contact resistance between graphene and metal NW is assumed to be 200 Ω·μm. (g) The simulated transmittance vs wavelength data for regular grating structures with periods of 5 and 10 μm, a line width of 100 nm, and a height of 100 nm. The average transmittances for the TE and TM modes are considered here.

form a continuous percolating path between electrodes. A sharp potential drop at the grain boundaries is observed for polygraphene samples (see the boxed regions in panels b and c of Figure 6), but the impact of high-resistance GBs is significantly suppressed in the hybrid system (Figure 6e,f). This occurs because a sparse metal NW mesh provides a low-resistance path to bypass high-resistance GBs.

It is clear from the discussion above that the sheet conductivity of polygraphene can be increased by doping it with a small number of Ag NWs, but does the approach compromise optical transmittance? For computational simplicity, we approximate the random NW dispersion with a regularized network (with the same spacing and the same dimensions of NW). Figure 6g shows the simulated transmittance for regular grating structures with a period of 10 μm, a line width of 100 nm, and a height of 100 nm, corresponding to a coverage of 100% (ρ_{NW} = 100%). The average transmittance (of the TE and TM modes) exceeds 99%, i.e., $T_{Ag} > 0.99$. Given that the transmittance of monolayer polygraphene is close to 97.7% as well, a graphene−NW composite is expected to achieve $T = T_{graphene}T_{Ag} \sim 0.96$. As shown in Figure 1, even with two to three layers of graphene, $T = (T_{graphene}T_{Ag})^{n(=2-3)} > 0.90$ is obtained.

These R_S and T values of NW-doped polygraphene suggest significant improvement of the trade-off between R_S and T for the NW-doped polygraphene as compared to conventional TCMs. There is an additional improvement: the NW-doped graphene also has reduced statistical variation in sheet resistance compared to pure polygraphene films. The inset of Figure 5 shows the normalized standard deviation (NSD) computed for polycrystalline graphene and the hybrid with $R_C \approx 200$ and 20 Ω·μm as a function of P_{GB}. For a polycrystalline graphene, the maximum NSD is about 0.15, which means about 15% variation in sheet resistance among the samples. The inset figure shows that NSD values for the hybrid with $R_C \approx 200$ Ω·μm are significantly improved. For $P_{GB} \approx 35\%$, an 4× reduction of NSD is achieved. It is clear that a metal NW mesh can suppress variation.

Recently, the concept of a metal NW−graphene composite has been experimentally demonstrated.[34] The experimental results are promising, but the two approaches are quite different. Zhu et al. use graphene to enhance the performance of a metallic grid defined by top-down photolithography with spacing much larger than grain sizes; the graphene provides a continuous conductive surface for the metallic grid. In contrast, we propose to randomly disperse a thin, subpercolating network of metallic tubes to enhance the performance of a graphene conductor by opening up new conducting channels through high-resistance GBs. Our assumptions that (i) the net transmission can be expressed as a product of transmittance of individual layers and that (ii) a highly conducting metal grid can change the effective sheet resistivity of graphene from kΩ/sq to ∼100 Ω/sq are clearly demonstrated by Figure 2c and Table 1 of ref 34. The two approaches have different trade-offs. The metallic grid-based approach may provide lower sheet resistance, while the NW-doped graphene-based approach being proposed here may provide greater transmission and (substrate) flexibility.

In summary, the impact of the microstructure on electrical performance of the large-area polycrystalline graphene has been numerically explored based on experimentally reported parameters such as grain shape, grain size, statistical distributions, and grain and grain boundary resistances. The numerical results show that the grain shape and its grain size distribution do not substantially affect the electronic performance, but the grain size and the percentage of high-resistance grain boundaries play important roles. We propose a novel concept of NW doping of polygraphene by Ag NWs to beat the transparency-conductivity constraint of pure polygraphene or pure NW networks. Our results show that both the sheet resistance and its variation can be significantly improved by using the hybrid without a loss of transmittance. These results should inspire new experiments in search of novel alternatives to transparent conducting oxides.

■ ASSOCIATED CONTENT

Supporting Information. Additional information on the process model, electrical model, optical model, and contact resistance dependence at NW density of 100%. This material is available free of charge via the Internet at http://pubs.acs.org.

■ AUTHOR INFORMATION

Corresponding Author

*E-mail: jeong.changwook@gmail.com; alam@purdue.edu.

■ ACKNOWLEDGMENT

This work was supported by the Focus Center Research Program (FCRP-MSD). Computational resources were provided

by the Network for Computational Nanotechnology (funded by the National Science Foundation under Cooperative Agreement No. EEC-0634750). P.N. and M.K. was supported by the Center for Re-Defining Photovoltaic Efficiency through Molecule Scale Control, an Energy Frontier Research Center funded by the U.S. Department of Energy, Office of Science, and Office of Basic Energy Sciences under Award Number DE-SC0001085. C.J. acknowledges discussions with D. Berdebes, E. Islam, L. Jauregui, and Y. Chen.

REFERENCES

(1) Hu, Y. H.; Wang, H.; Hu, B. *ChemSusChem* **2010**, *3*, 782–796.
(2) Hu, L.; Hecht, D. S.; Grüner, G. *Appl. Phys. Lett.* **2009**, *94*, 081103–081105.
(3) Dongaonkar, S.; Servaites, J. D.; Ford, G. M.; Loser, S.; Moore, J.; Gelfand, R. M.; Mohseni, H.; Hillhouse, H. W.; Agrawal, R.; Ratner, M. A. *J. Appl. Phys.* **2010**, *108*, 124509–124517.
(4) Chandra, B.; Afzali, A.; Khare, N.; El-Ashry, M. M.; Tulevski, G. S. *Chem. Mater.* **2010**, *22*, 5179–5183.
(5) Geng, H.; Kim, K. K.; So, K. P.; Lee, Y. S.; Chang, Y.; Lee, Y. H. *J. Am. Chem. Soc.* **2007**, *129*, 7758–7759.
(6) Lee, J.; Connor, S. T.; Cui, Y.; Peumans, P. *Nano Lett.* **2008**, *8*, 689–692.
(7) Wu, H.; Hu, L.; Rowell, M. W.; Kong, D.; Cha, J. J.; McDonough, J. R.; Zhu, J.; Yang, Y.; McGehee, M. D.; Cui, Y. *Nano Lett.* **2010**, *10*, 4242–4248.
(8) Bae, S.; Kim, H.; Lee, Y.; Xu, X.; Park, J.; Zheng, Y.; Balakrishnan, J.; Lei, T.; Ri Kim, H.; Song, Y. I.; Kim, Y.; Kim, K. S.; Ozyilmaz, B.; Ahn, J.; Hong, B. H.; Iijima, S. *Nat. Nanotechnol.* **2010**, *5*, 574–578.
(9) Li, X.; Magnuson, C. W.; Venugopal, A.; An, J.; Suk, J. W.; Han, B.; Borysiak, M.; Cai, W.; Velamakanni, A.; Zhu, Y. *Nano Lett.* **2010**, *10*, 4328–4334.
(10) Li, X.; Cai, W.; An, J.; Kim, S.; Nah, J.; Yang, D.; Piner, R.; Velamakanni, A.; Jung, I.; Tutuc, E.; Banerjee, S. K.; Colombo, L.; Ruoff, R. S. *Science* **2009**, *324*, 1312–1314.
(11) Kim, K. S.; Zhao, Y.; Jang, H.; Lee, S. Y.; Kim, J. M.; Kim, K. S.; Ahn, J.; Kim, P.; Choi, J.; Hong, B. H. *Nature* **2009**, *457*, 706–710.
(12) Pimparkar, N.; Chowalla, M.; Alam, M. A. *IEEE Photovoltaic Spec. Conf., 33rd* **2008**, 1–4.
(13) De, S.; King, P. J.; Lyons, P. E.; Khan, U.; Coleman, J. N. *ACS Nano* **2010**, *4*, 7064–7072.
(14) De, S.; Coleman, J. N. *ACS Nano* **2010**, *4*, 2713–2720.
(15) Pimparkar, N.; Cao, Q.; Rogers, J. A.; Alam, M. A. *Nano Res.* **2009**, *2*, 167–175.
(16) Okabe, A.; Boots, B.; Sugihara, K.; Chiu, S. N. *Spatial tessellations: Concepts and Applications of Voronoi Diagrams*; John Wiley and Sons: Chichester and New York, 2000.
(17) Yu, Q.; Jauregui, L. A.; Wu, W.; Colby, R.; Tian, J.; Su, Z.; Cao, H.; Liu, Z.; Pandey, D.; Wei, D. *Nat. Mater.* **2011**, *10*, 443–449.
(18) Huang, P. Y.; Ruiz-Vargas, C. S.; van der Zande, A. M.; Whitney, W. S.; Levendorf, M. P.; Kevek, J. W.; Garg, S.; Alden, J. S.; Hustedt, C. J.; Zhu, Y.; Park, J.; McEuen, P. L.; Muller, D. A. *Nature* **2011**, *469*, 389–392.
(19) Nemes-Incze, P.; Yoo, K. J.; Tapaszto, L.; Dobrik, G.; Labar, J.; Horvath, Z. E.; Hwang, C.; Biro, L. P. *Appl. Phys. Lett.* **2011**, *99*, 023104–923106.
(20) Bolotin, K. I.; Sikes, K. J.; Hone, J.; Stormer, H. L.; Kim, P. *Phys. Rev. Lett.* **2008**, *101*, 096802–096804.
(21) Yazyev, O. V.; Louie, S. G. *Nat. Mater.* **2010**, *9*, 806–809.
(22) Multiphysics and Simulation Software: COMSOL. http://www.comsol.com/.
(23) Hsu, H.; Huang, M. *Phys. Rev. E* **1999**, *60*, 6361–6370.
(24) Becker, A. M.; Ziff, R. M. *Phys. Rev. E* **2009**, *80*, 041101–041108.
(25) Sykes, M. F.; Essam, J. W. *J. Math. Phys.* **1964**, *5*, 1117–1127.
(26) Pike, R.; Stanley, H. E. *J. Phys. A: Math. Gen.* **1981**, *14*, L169–L177.
(27) McLachlan, D. S.; Blaszkiewicz, M.; Newnham, R. E. *J. Am. Ceram. Soc.* **1990**, *73*, 2187–2203.
(28) Rossi, E.; Adam, S.; Das Sarma, S. *Phys. Rev. B* **2009**, *79*, 245423–245429.
(29) Straley, J. P. *Phys. Rev. B* **1977**, *15*, 5733–5737.
(30) Frank, D. J.; Lobb, C. J. *Phys. Rev. B* **1988**, *37*, 302–307.
(31) Hsu, A.; Wang, H.; Kim, K. K.; Kong, J.; Palacios, T. *IEEE Electron Device Lett.* **2011**, *32*, 1008–1010.
(32) Berdebes, D.; Low, T.; Sui, Y.; Appenzeller, J.; Lundstrom, M. arXiv:1103.5773v2, 2011.
(33) Giovannetti, G.; Khomyakov, P. A.; Brocks, G.; Karpan, V. M.; van den Brink, J.; Kelly, P. J. *Phys. Rev. Lett.* **2008**, *101*, 026803–026806.
(34) Zhu, Y.; Sun, Z.; Yan, Z.; Jin, Z.; Tour, J. M. *ACS Nano* **2011**, *5*, 6472–6479.
(35) Cao, Q.; Kim, H.; Pimparkar, N.; Kulkarni, J. P.; Wang, C.; Shim, M.; Roy, K.; Alam, M. A.; Rogers, J. A. *Nature* **2008**, *454*, 495–500.
(36) Chen, J.-H.; Jang, C.; Xiao, S.; Ishigami, M.; Fuhrer, M. S. *Nat. Nanotechnol.* **2008**, *3*, 206–209.
(37) Kumar, S.; Murthy, J. Y.; Alam, M. A. *Phys. Rev. Lett.* **2005**, *95*, 066802.